

Electrochemical Impedance Spectroscopy to Evaluate the Effect of Pressure Exerted in the Hot-Pressing Stage on the Performance of PEMFC

Fu-Pin Ting¹, Jing-Chie Lin^{1,2,*}, Chien-Ming Lai³, San-Der Chyou⁴, Kan-Lin Hsueh⁵

¹ Department of Mechanical Engineering, Central University, Jhongli city, Taiwan

² Institute of Materials Science and Engineering, National Central University, Jhongli city, Taiwan

³ Material and Chemical Research Laboratories, Industrial Technology Research Institute, Hsinchu, Taiwan

⁴ Taiwan Power Research Institute, Taiwan Power Company, New Taipei City, Taiwan

⁵ Department of Energy and Resources, National United University, Miaoli City, Taiwan

*E-mail: jclin4046@gmail.com

Received: 25 June 2012 / Accepted: 16 July 2012 / Published: 1 August 2012

Hot-pressing is one of the most important stages in fabrication of the membrane electrode assembly in a single cell of proton exchange membrane fuel cells (PEMFCs). Electrochemical impedance spectroscopy (EIS) is one of the most powerful nondestructive tools used to evaluate the performance of PEMFCs. This study focused on the pressure exerted during the hot-pressing stage of construction of a single cell. EIS data were analyzed and simulated by an equivalent circuit including elements such as internal impedance (R_s), interfacial impedance (R_{if}), and reaction impedance (R_{rxn}). We found that the ohmic resistance derived from I-V diagrams is equal to the sum of R_s and R_{if} . R_{if} can be isolated from ($R_s + R_{if}$) for use as an evaluation criterion by performing cyclic voltammetry and linear sweep voltammetry. R_{if} is related to the three-phase interfacial reaction (i.e., catalyst-electrolyte-reactant) that is important in evaluating the effects of hot-pressing pressure on the performance of PEMFCs.

Keywords: proton exchange membrane fuel cell (PEMFC); electrochemical impedance spectroscopy; hot-pressing pressure; gas diffusion; reaction impedance

1. INTRODUCTION

Proton exchange membrane fuel cells (PEMFCs) have recently been developed to provide clean energy by conversion of chemical energy into electricity. PEMFCs have low emissions, high power density, a relatively simple design, quick start up, low noise emissions, and high-energy

conversion efficiency (40%–60%) compared to traditional power sources. It is believed that PEMFCs be applied in the fields of portable 3C products, military equipment, transportation devices, and stationary or dispersion power stations [1-7]. Hot pressing is a simple method generally adopted to assemble the components of membrane electrode assemblies MEAs to form PEMFCs. Many parameters such as temperature, pressure, and duration of the hot pressing process are considered to influence the performance of PEMFCs. We reviewed a number of papers [8-23] and defined appropriate ranges for the parameters of the hot-pressing process: temperature should be within the range 80–155°C, pressure within the range 2–155 kg cm⁻², and duration within the range 50–300 s. Few papers have studied MEA preparation where the parameters are not within these ranges. Yin et al [18] reported that a higher pressure (e.g., at 160 kg cm⁻²) applied during hot pressing causes damage to the carbon paper, thus reducing conductivity in the MEA. Moreover, in another study that discussed the choices of improper combinations of hot-pressing parameters, the MEA led to poor performance due to a thinning of the conductive layer arising from deep embedding of catalysts in the electrolyte membrane [19]. Zhao and his coworkers [20] found that the durability of MEAs could be improved by increasing the hot-pressing time (i.e., 60 min rather than 3 min). The improvement of MEA durability is ascribed to stronger binding at the interfaces between the electrodes and membrane. This stronger binding may suppress delamination of the catalyst from the electrolyte membrane.

An I-V curve is one of the common methods of evaluating the performance of PEMFCs. Current density in the I-V diagram is used to estimate the performance of PEMFCs with the same range in voltage drop. The voltage drop in the I-V diagram reveals three characteristic regions: the active, ohmic, and mass-transfer limiting regions [24-27].

Electrochemical impedance spectroscopy (EIS) is a powerful tool used to explore electrochemical kinetic and reaction mechanism [28]. In a paper reviewed by Wang and coworkers [29], EIS was reported to provide useful information by analysis of inner structures (catalyst layer, gas diffusion layer, or thickness of electrolyte membrane) of PEMFCs, to interpret the effect of reaction accretion (i.e., loading amount of the catalyst or of Nafion solution) and the possible poisoning mechanism (CO or H₂S) involved. In our previous work [30-32], we used EIS to study the reaction mechanism of DEMFCs and PEMFCs. A model of equivalent circuit was proposed to elucidate the electrochemical kinetics. According to the equivalent circuit, the impedance data could be divided into three categories: high-frequency impedance at the catalyst–Nafion ionomer interface, medium-frequency impedance as a result of electrochemical reactions, and low-frequency impedance caused by adsorption/relaxation of CO. This model was modified and found to fit the electrochemical kinetics performed in the PEMFC [31-32]. We concluded that interfacial impedance (R_{if}) is a critical model element.

In the present study, we investigate the effect of hot-pressing pressure on catalytic activity and cell performance. I-V polarization and EIS were used to estimate performance of the cells. Additional experiments were carried out by using cyclic voltammetry (CV), linear sweep voltammetry (LSV), scanning electron microscopy (SEM), and measurement of gas permeability to confirm the proposed reaction mechanism based on the I-V diagram and EIS model.

2. EXPERIMENTAL DETAILS

2.1. Preparation of the electrodes/MEA

MEAs (membrane electrode assemblies) supply power for PEMFCs and comprise a proton exchange membrane sandwiched between two gas diffusion electrodes. The gas diffusion electrodes (GDE, LT-120EW) consist of a thin gas diffusion layer coated with Pt-catalyst (E-TEK). The major component of the gas diffusion layer is carbon cloth with an electrocatalyst layer (30 wt% Pt/Vulcan XC-72 carbon black; $112 \text{ m}^2 \text{ g}^{-1}$ surface area; E-TEK), coated with Pt-loading of 0.5 mg cm^{-2} . The surface of the GDE was sprayed with a solution of Nafion (containing 5 wt% Nafion ionomers) and dried overnight in an oven at 80°C to assure the uniform loading of Nafion at 1.0 mg cm^{-2} . This process of spraying and drying increases the conduction path for H^+ ions, thus improving catalyst utilization [33].

Nafion 112 (DuPont) was used as the proton exchange membrane. Each new membrane was immersed in a bath of 10% hydrogen peroxide to boil for 8 h, removing organic contaminants, and then boiled in deionized water (DI) for 2 h and in 1 M sulfuric acid for 8 h to remove metallic impurities and ensure its H-form. The membrane was rinsed in boiling DI water for 2 h before use.

A specimen of full-cell was fabricated by placing one piece of Nafion 112 between two pieces of GDE (acting as either anode or cathode, with an active area of 10.89 cm^2 for each GDE). Assembly was performed in a hot press with temperature maintained at 125°C for 3 min under varying pressure (50 Kg cm^{-2} , 80 Kg cm^{-2} , 100 Kg cm^{-2} , and 130 Kg cm^{-2}) and removed to cool. A sample of half-cell electrode was prepared in the same way, but with one piece of GDE.

2.2. Evaluation of electrodes/MEA

2.2.1 Measurements of I–V polarization

A testing station (Beam Inc., Taiwan), consisting of a temperature controller, humidification chamber, mass flow meter, and electronic load (10 V, 60 A), was employed to conduct I–V polarization measurements for the single cell. Current was recorded under a series loading of voltages, from the open circuit potential (OCP) to 0.25 V in 25 mV increments and maintained at each voltage level for 30 s. During measurement, the anode was fed with humid hydrogen (with a stoichiometry of 1.5 at 75°C), and the cathode was fed with humid air (with a stoichiometry of 2.0 at 65°C). The temperature of the PEMFC was maintained at $60.0^\circ\text{C} \pm 0.1^\circ\text{C}$ and the operational pressure was fixed at ambient atmosphere.

2.2.2 Measurement of EIS

A galvanostat/potentiostat (AutoLab PGSTAT30, ECO Chemie BV, Netherlands) equipped with a frequency response analyzer (FRA2 module) was employed to carry out the EIS measurement for the single cell under open circuit potential. The original anode acted as a reference (dynamic

hydrogen electrode (DHE)) and was coupled with the counter electrode to connect the electrometer. The cathode of the cells to be tested was connected to the working electrode of the potentiostat. The impedance spectra were measured potentiostatically, with input sine waves with amplitude of 10 mV, from 20 kHz to 10 mHz (high frequency to low frequency). Analysis and curve fitting of the data were done with Z-View software. The testing conditions for EIS were maintained for I-V polarization.

2.2.3 Estimation of catalytic activity by cyclic voltammetry

CV was used to estimate the catalytic activity of the electrodes with a galvanostat/potentiostat. Specimens of half-cell PEMFC were estimated in a cell filled with 0.5 M H₂SO₄ under a three-electrode mode. A Pt-foil (with 99.99% purity) served as the counter-electrode, and a saturated calomel electrode (SCE) coupled with the Luggin-Haber probe as the reference. Nitrogen gas (N₂) was continuously purged (with a flow rate of 150 ml min⁻¹) on the backside of the electrode to avoid interference from oxygen reduction. In the absence of oxygen reduction, the electrochemical reactions are confined to the two-phase interfacial region between the catalyst and the electrolyte [31, 32]. Only hydrogen was adsorbed on the two-phase interfacial region. The CV plots were performed at 25°C ± 0.1°C with a scan rate of 20 mV s⁻¹ at a potential increasing from 50 to 1,400 mV (vs. standard hydrogen electrode, SHE) then inverted. Ten runs of CV experiments were conducted under the same conditions to ensure reproducibility.

2.2.4 Estimation of oxygen reduction reaction (ORR) by linear sweep voltammetry

LSV was used to estimate ORR with the galvanostat/potentiostat. The experimental setup and testing conditions for the LSV study is similar to those employed in the CV technique but purging with air instead of nitrogen gas. This method explores reactions taking place at the three-phase interfaces where ORR is involved due to the presence of oxygen. The LSV plots were constructed by scanning the potential in the range from 1.000 V to 0.050 V with a scan rate of 20 mV s⁻¹ under the same conditions as the CV method.

2.3. Characterization of the GDE

Specimens of GDE were characterized by their surface morphology and subjected to gas permeability measurements. The surface morphology was examined by scanning electron microscopy (SEM, HITACHI S-3500). Gas permeability of the GDE specimens was measured using a capillary flow porometer (CFP-1500A, Porous Materials, Inc., Ithaca, New York, USA). The specimens were prepared as described in section 2.1. The gas permeability was determined directly by estimating the pressure difference between two sides of the testing specimen, feeding air to maintain 100 psi at one end.

3. RESULTS AND DISCUSSION

3.1. Effect of hot-pressing pressures on the I–V diagram

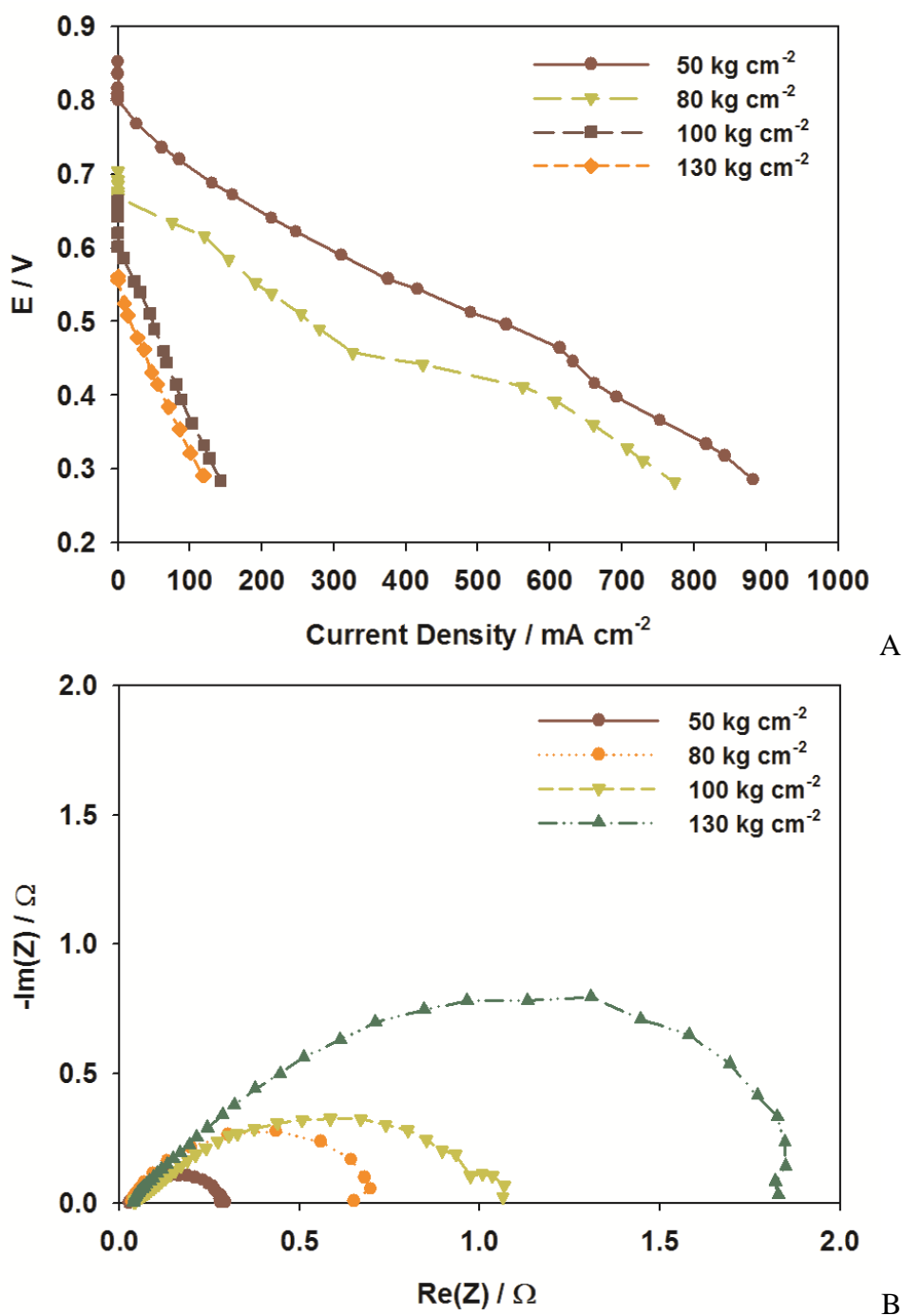


Figure 1. I-V polarization diagram (a) and Nyquist plot (b) for the MEA specimens prepared at hot-pressing pressures of 50, 80, 100, and 130 Kg cm^{-2} .

Figure 1(a) depicts the I-V diagram at 60°C for various MEA specimens fabricated with different hot-pressing pressures. The relationship between E and current density depends upon the pressure. The magnitude of current density discharged at constant voltages was compared to evaluate

the performance of the MEAs. For instance, for a voltage of 0.4V, the current density discharged in different MEAs was different. Increasing the pressure from 50 Kg cm⁻² to 130 Kg cm⁻² resulted in the current density discharged decreasing from 692 mA cm⁻² to 69 mA cm⁻². It is preferable to choose 50 Kg cm⁻² rather than 130 Kg cm⁻² in the hot-pressing process.

It is generally accepted that the voltage drop in the I-V diagram can be resolved into three regions caused by active, ohmic, and mass-transfer limiting polarization. The overall potential for this system can be estimated by consideration of various polarizations departing from the equilibrium potential as follows [25]:

$$E = E_0 - b \log i - i R_Q - m \exp(ni) \tag{1}$$

where E indicates the overall voltage for the full-cell, and E_0 is the open circuit potential for the full-cell. b is the Tafel slope, and $b \log i$ is a Tafel term resulting from activation polarization leading to a sudden voltage drop. R_Q is the resistance between the electrode and electrolyte, and $i R_Q$ is the linear potential drop term derived from ohmic resistance (R_Q). The final term $m \exp(ni)$, where m and n are parameters with the units of potential and the reciprocal of current density, respectively, is responsible for potential loss arising from concentration polarization. Kim et al. [24] reported that the contribution to mass-transport limitations is greater for parameter n than m . In addition, m is more significant in increasing the slope of linear region in the plot of E vs. i that is governed by concentration polarization.

3.2. Effect of the hot-pressing pressures on EIS

Figure 1(b) displays the Nyquist plots at open circuit potentials (OCPs) at 60°C for various MEAs prepared by varying pressure from 50 to 130 Kg cm⁻² during hot pressing. Distortion of the capacitive loop can be ascribed to variation in impedance contributed by different elements of the equivalent circuit. The diameter estimated from the distorted capacitive semicircle was evaluated for various MEAs.

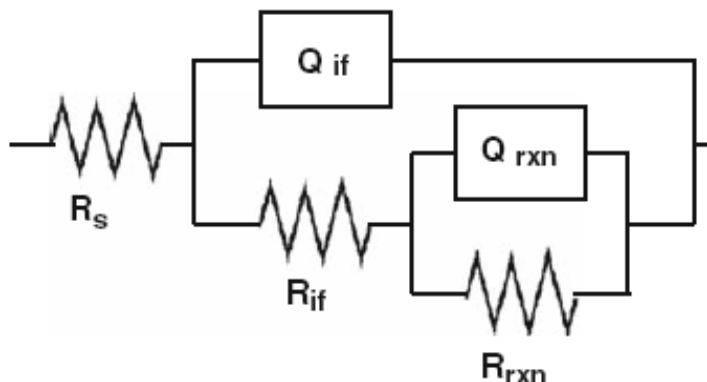


Figure 2. The equivalent circuit mode for the proton exchange membrane fuel cell.

A smaller diameter indicates better performance of the cell. The intersection between the horizontal axis and the capacitive loop at the highest frequencies determines the internal resistance of the cell, R_s . R_s remained constant (ca. 0.03Ω) despite varying hot-pressing pressures. In contrast, the diameter responsible for the distorted semicircle tends to increase with increasing hot-pressing pressure. The MEA specimen prepared at 50 Kg cm^{-2} reveals the distorted semicircle with the smallest diameter, whereas that prepared at 130 Kg cm^{-2} reveals the distorted semicircle with the largest diameter.

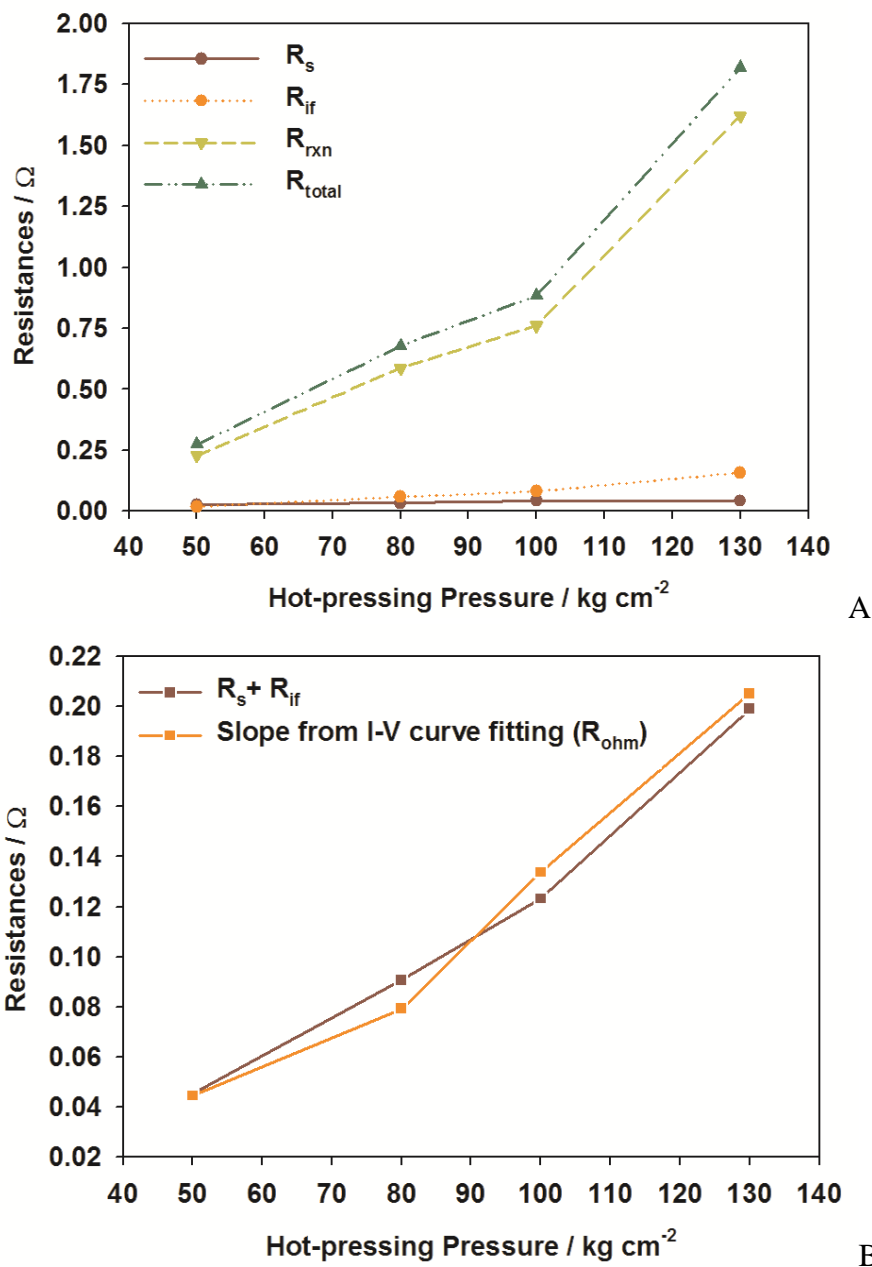


Figure 3. (a) The data of resistance estimated by simulation of equivalent circuits and (b) a comparison of the dependence on hot-pressing pressure of R_{Ω} , estimated from the I-V diagram, with that for $(R_s + R_{if})$, a combination of R_s and R_{if} data estimated from electrochemical impedance spectroscopy.

In our previous work [30-32], we tried to verify the present system. Figure 2 is the equivalent circuit model consisting of an element of R_s and two circuits including R_{if}/Q_{if} and R_{rxn}/Q_{rxn} . R_s is ascribed to internal impedance coming from PEMFC; R_{if}/Q_{if} is responsible for the interfacial reaction in PEMFC and R_{rxn}/Q_{rxn} corresponds to an electrochemical reaction. Capacitance (C) is the element commonly used in the conventional equivalent circuit model. In the case of a porous specimen with rough surface, the use of a constant phase element (CPE, Q) in place of C is preferred. In this work, CPE is used since the specimens are porous. Our treatment is consistent with Hsu's work [34] in which CPE was instead of C to obtain better agreement between the experimental data and theoretical calculations.

Figure 3(a) depicts a plot of data for resistances (i.e., R_s , R_{if} , R_{rxn} , and R_{total}) estimated by simulation of equivalent circuits shown in Figure 2 against the hot-pressing pressures. Figure 3(a) shows that R_s remains constant (ca. 0.03 Ω) in spite of increasing pressure, implying that increases in the hot-pressing pressure have no influence on the internal resistance of PEMFCs. R_{if} increases from 0.02 Ω at 50 Kg cm⁻² to 0.16 Ω at 130 Kg cm⁻². R_{rxn} increases from 0.23 Ω at 50 Kg cm⁻² to 1.62 Ω at 130 Kg cm⁻² and is supposedly related to the ease of diffusion of gases and their electrochemical reactions. R_{total} is dominated by R_{if} and R_{rxn} .

It is important to correlate the resistance data to the related polarizations in PEMFCs [31-32]. Figure 3(b) compares the dependence of hot-pressing pressure for R_{Ω} , estimated from I-V diagram, with that for $(R_s + R_{if})$, estimated from EIS. Linear regression of the data in Figure 1(a) reveals similar curves. As previously mentioned, R_s is independent of pressure, inferring that R_{if} is a critical term that depends upon pressure and makes an important contribution to ohmic polarization in PEMFCs. Although R_{if} is of lower magnitude than R_{rxn} , they exhibit a similar trend (Figure 3(a)). It is of concern whether the ohmic polarization results from two-phase interfacial reaction (i.e., catalyst-electrolyte) or three-phase interfacial reaction (i.e., catalyst-electrolyte-reactant). R_{if} may provide a criterion to select between them and allow diagnosis of catalytic activity in PEMFCs.

3.3. Catalytic activity estimated by CV

We estimated the catalytic activity of the specimen made of Pt/C powder by integrating the area of the characteristic reduction peak. Figure 4(a) demonstrates CV voltammograms for various MEAs (half-cell) prepared at 50, 80, 100, and 130 Kg cm⁻² in the hot-pressing process by half-cell testing. The activity of the catalyst was evaluated by integrating the area for the anodic peak responsible for hydrogen adsorption in the range from 0.05 to 0.4 V (vs. SHE). A peak with greater area indicates that the catalyst has higher activity. In Figure 4(a), the area corresponding to hydrogen reduction is similar for all specimens. Therefore, pressure variation during hot pressing causes no significant change in the performance of the activity of the Pt/C catalyst.

The catalytic activity of the half-cell electrode can be estimated by CV in terms of electrochemical surface area (ECSA). The ECSA of the catalyst is calculated using the following equation [35].

$$\text{ECSA (m}^2\text{ g}^{-1}) = \frac{\text{Charge area (}\mu\text{C cm}^{-2}\text{)}}{10 \times 220 (\mu\text{C cm}^{-2}) \times \text{Catalyst loading (mg cm}^{-2}\text{)}} \quad (2)$$

In Eq (2), the Pt-catalyst is responsible for the adsorption of hydrogen in the CV plot indicated by a broad peak. The charge area under the peak of H₂-adsorption can be integrated by subtracting the nonfaradaic charge from the anodic peak.

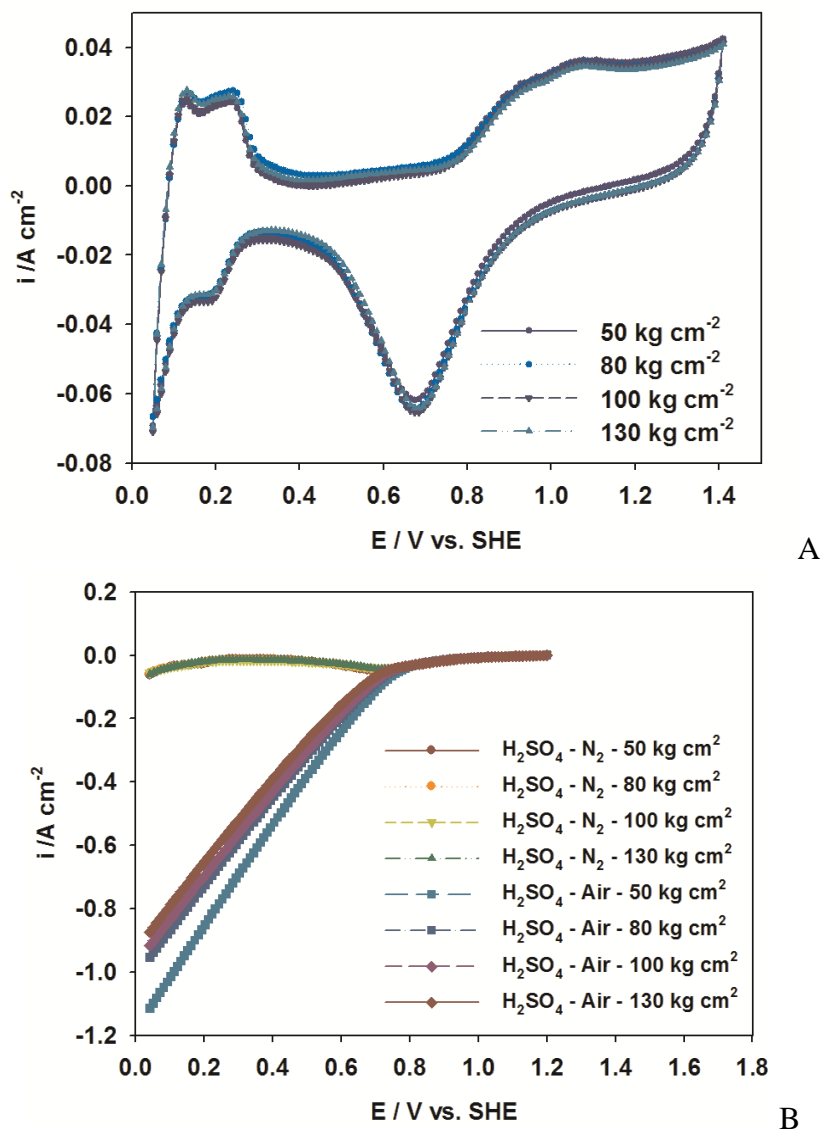


Figure 4. (a) Cyclic voltammetry plot and (b) linear sweep voltammetry curves for the membrane electrode assembly prepared at hot-pressing pressures of 50, 80, 100, and 130 Kg cm⁻² by half-cell testing.

The value $10 \times 220 (\mu\text{C cm}^{-2})$ is the charge required for adsorption of atomic hydrogen on the smooth Pt-surface. The ECSA estimated from CV curves using Eq (2) can be compared to the hot-pressing pressure. ECSA remains at about $19 \text{ m}^2 \text{ g}^{-1}$, despite variations in pressure. This implies that

the activity of catalysts is independent of hot-pressing pressures. CV was conducted in the absence of oxygen so that only hydrogen reduction plays a role on the two-phase interfacial region. This reduction is confined to the two-phase interfacial region between the catalyst and the electrolyte [31].

3.4. Activity of ORR evaluated by LSV

Figure 4(b) displays LSV curves for ORRs of half-cell testing of various specimens. LSV provides a convenient estimation of the activity of the catalyst under ORR. No reduction current was found for all specimens under purging with nitrogen gas; however, current could be detected in the presence of air or oxygen. This phenomenon reflects the fact that LSV is a sensitive test for ORR. The on-set potentials are almost the same for all the specimens despite variations in pressure. Fixing the potential at 0.4 V reduces the current density for ORR from 0.53 A cm^{-2} (50 Kg cm^{-2}) to 0.38 A cm^{-2} (130 Kg cm^{-2}). The specimen prepared at 50 Kg cm^{-2} reveals higher activity than those prepared at higher pressures.

For ORR, activity can be evaluated by LSV. In contrast to CV, which provides estimation of catalytic activity for two-phase interfacial reactions, LSV allows estimation of three-phase interfacial reaction (catalyst-electrolyte-reactant). For LSV, a reduction current ($\Delta i_{red} = i_{red,Air} - i_{red,N_2}$) for ORR should be calculated for comparison. From Figure 4(b), the reduction current is negligible under purging with N_2 for the half-cell electrode. On the other hand, the reduction current caused by a constant feed of air into the half-cell electrode varies in magnitude depending on the hot-pressing pressure. By holding the current density at 0.4 V, we found that current density for ORR has a maximum value of -0.53 A cm^{-2} at 50 Kg cm^{-2} and decreases with increasing hot-pressing pressure. R_{if} estimated by EIS displays the same reliance on hot-pressing pressure as the polarization resistance, derived from LSV plot. Both are believed to be intimately associated with three-phase interfacial reactions occurring on the interface of catalyst-electrolyte-reactant.

3.5. Structure and gas permeability of GDE

Figure 5 depicts SEM morphologies for various specimens of GDE prepared at different hot-pressing pressures. It is obvious that pores are present on the specimens prepared at lower pressure (e.g., at 50 , 80 and 100 Kg cm^{-2}). However, many fewer are found on the specimens prepared at higher pressure (e.g., 130 Kg cm^{-2}). It is believed that specimens prepared under lower pressures retain more space, resulting in higher porosity, while specimens prepared under higher pressures lead to compact structures and lower porosity.

Figure 6 illustrates gas permeability curves for various specimens of GDE, as determined by the porometer. We found that gas permeability (D) decreases with increasing hot-pressing pressure. D decreases from $3.4 \times 10^{-3} \text{ D}$ at 50 Kg cm^{-2} to $2.0 \times 10^{-3} \text{ D}$ at 130 Kg cm^{-2} , about a decrease of $1.4 \times 10^{-3} \text{ D}$ with increasing pressure. This decrease in gas permeability may arise from the compact structure of the specimen that hinders the movement and diffusion of the gas. This can be expressed quantitatively by the pressure drop.

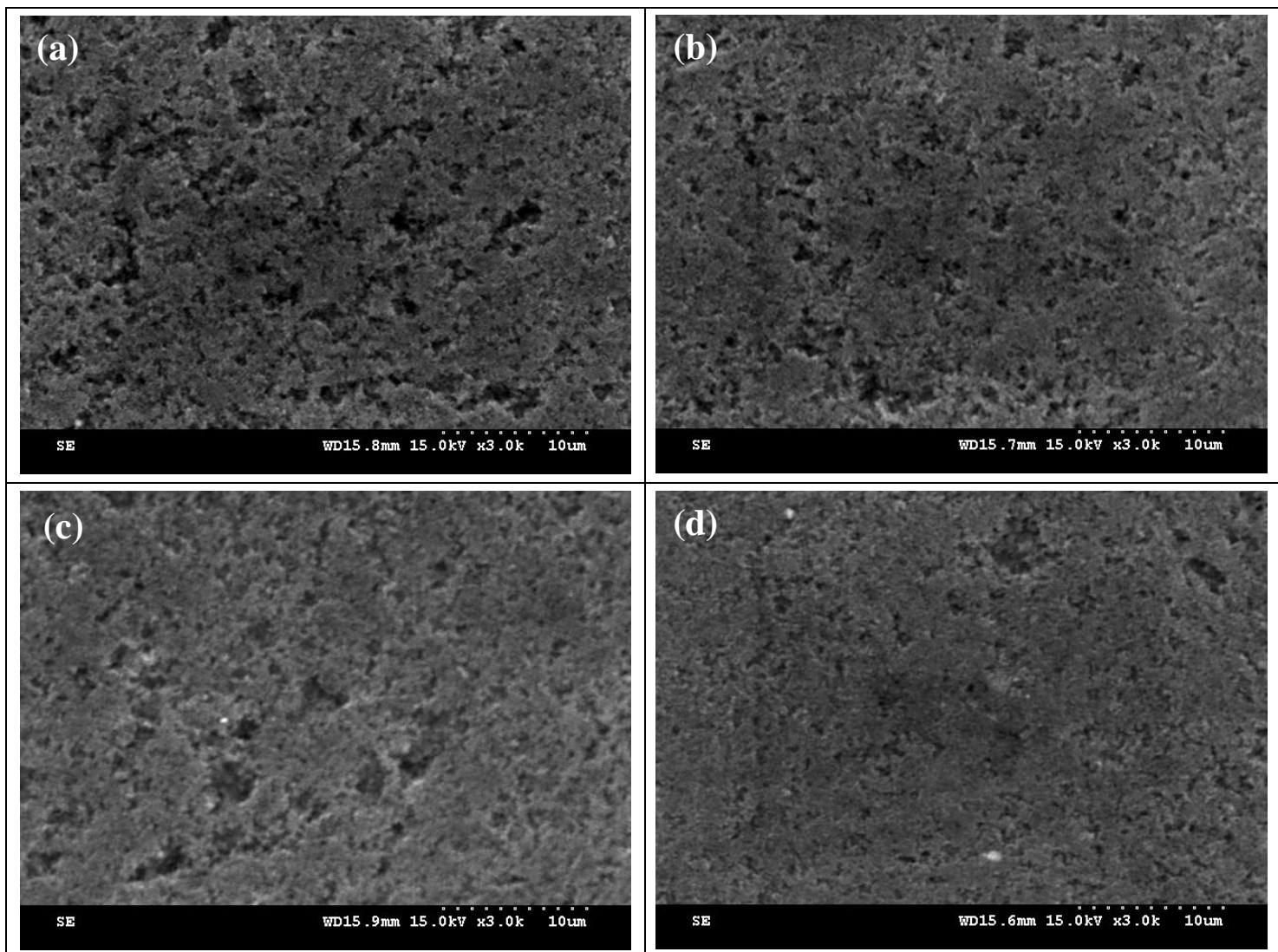


Figure 5. SEM morphologies of the specimen gas diffusion electrodes prepared at (a) 50, (b) 80, (c) 100, and (d) 130 Kg cm⁻² by the hot-pressing process. (3000 X)

The SEM morphologies shown in Figure 5 indicate that the structure of GDE specimens is porous, providing channels for diffusion of the feeding gases. The SEM structure indicates increasing compactness with increasing hot-pressing pressure (from 50 to 130 Kg cm⁻²). Quantitatively, D decreases from 3.4×10^{-3} D at 50 Kg cm⁻² to 2.0×10^{-3} D at 130 Kg cm⁻². With reference to R_{if} and R_{rxn} , it could be concluded that a more compact structure reflects lower gas permeability but higher impedance. In Section 3.4, we infer that the electrochemical reaction of ORR occurs at three-phase interfaces and depends upon the behavior of R_{if} in response to pressure, as described in Figure 3(a). As a result, the compactness of the GDE specimens is enhanced by increasing hot-pressing pressure. This hinders the permeation of feeding gases and increases the magnitude of R_{if} to hinder the three-phase interfacial reaction. This result is consistent with the previous study [18] that provided no mechanistic information.

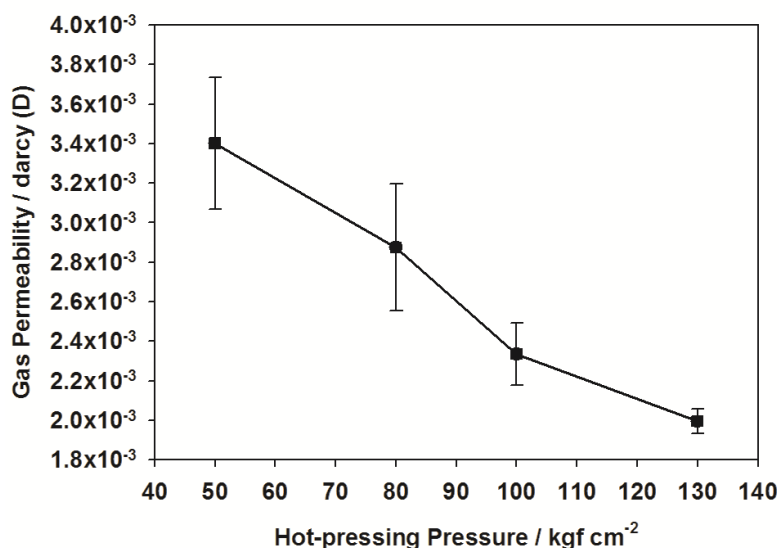


Figure 6. Gas permeability curves for the specimen gas diffusion electrodes prepared at various hot-pressing pressures.

4. CONCLUSIONS

In manufacturing of PEMFCs, hot-pressing is a key process in the preparation of MEAs. Optimal control of parameters such as temperature, pressure, and duration is of significance. This study undertook a systematic investigation to study the effect of hot-pressing pressure on the performance of half-cell and full-cell PEMFCs. The optimal operational conditions for hot-pressing pressure were 50 Kg cm⁻².

EIS offered a means of interpreting the electrochemical mechanism for the performance of the testing cells. By simulating the equivalent circuit, we attained three characteristic parameters to delineate the theoretical background for the effect of hot-pressing pressure on the performance of PEMFCs: internal resistance (R_s), interfacial resistance (R_{if}), and reaction resistance (R_{rxn}).

In studying the role of these resistance parameters, we discovered that ohmic resistance derived from an I-V diagram is equal to the sum of R_s and R_{if} . With the aid of CV and LSV techniques, R_{if} can be isolated and used as an evaluation criterion, which is related to the three-phase interfacial reaction (i.e., catalyst-electrolyte-reactant) and allows for evaluation of the effect of hot-pressing pressure on the performance of PEMFCs. A constant ECSA (i.e., 19 m² g⁻¹) estimated by CV provided the justification for ruling out the contribution of two-phase interfacial reaction (i.e., catalyst-electrolyte) to R_{if} . The mechanistic information was confirmed qualitatively by examining SEM morphology and quantitatively by gas permeability measurements.

ACKNOWLEDGEMENTS

We gratefully acknowledge the financial support by the Taiwan Power Research Institute, Taiwan Power Company, under contract number T5469410021 and the National Science Council of Taiwan under contract No.: NSC 101-3113-P-008-006.

References

1. Keith B. Prater, *J. Power Sources*, 51 (1994) 129.
2. Keith B. Prater, *J. Power Sources*, 61 (1996) 105.
3. S.J.C. Cleghorn, X. Ren, T.E. Springer, M.S. Wilson, C. Zawodzinski, and T.A. Zawodzinski, et al., *Int. J. Hydrogen Energy*, 22 (1997) 1137.
4. Paola Costamagna and Supramaniam Srinivasan, *J. Power Sources*, 102 (2001) 242.
5. Fritz R. Kalhammer, Consultant and Vernon P. Roan, *Transportation Applications for Fuel Cells*, Encyclopedia of Physical Science and Technology (Third Edition) (2004) 107.
6. H.-J. Neef, *Energy*, 34 (2009) 327.
7. Yun Wang, Ken S. Chen, Jeffrey Mishler, Sung Chan Cho and Xavier Cordobes Adroher, *Applied Energy*, 88 (2011) 981.
8. J.M. Song, S.Y. Cha and W.M. Lee, *J. Power Sources*, 94 (2001) 78.
9. Sergei Gamburgzev and A. John Appleby, *J. Power Sources*, 107 (2002) 5.
10. Han-Kyu Lee, Jong-Ho Park, Do-Young Kim and Tae-Hee Lee, *J. Power Sources*, 131 (2004) 200.
11. E.A. Cho, U.-S. Jeon, H.Y. Ha, S.-A. Hong and I.-H. Oh, *J. Power Sources*, 125 (2004) 178.
12. Young-Gi Yoon, Won-Yong Lee, Gu-Gon Park, Tae-Hyun Yang and Chang-Soo Kim, *Electrochim. Acta*, 50 (2004) 709.
13. Chan Lim and C.Y. Wang, *Electrochim. Acta*, 49 (2004) 4149.
14. Th. Frey and M. Linardi, *Electrochim. Acta*, 50 (2004) 99.
15. B. Yang, Y.Z. Fu and A. Manthiram, *J. Power Sources*, 139 (2005) 170.
16. Mu Pan, Hao Lin Tang, San Ping Jiang and Zengcai Liu, *Electrochemistry Communications*, 7 (2005) 119.
17. Haolin Tang, Shenlong Wang, San Ping Jiang and Mu Pan, *J. Power Sources*, 170 (2007) 140.
18. Jian Zhang, Ge-Ping Yin, Zhen-Bo Wang, Qin-Zhi Lai and Ke-Di Cai, *J. Power Sources*, 73 (2007) 73.
19. Apichai Therdthianwong, Phochan Manomayidthikarn and Supaporn Therdthianwong, *Energy*, 32 (2007) 2401.
20. Z.X. Liang, T.S. Zhao, C. Xu and J.B. Xu, *Electrochim. Acta*, 53 (2007) 894.
21. Haolin Tang, Shenlong Wang, Mu Pan, San Ping Jiang and Yunzhang Ruan, *Electrochim. Acta*, 52 (2007) 3714.
22. Juei Dong Lu and Ming-Chang Yang, *J. Power Sources*, 196 (2011) 8519.
23. Perumal Bhavani, and Dharmalingam Sangeetha, *Int. J. Hydrogen Energy*, 36 (2011) 14858.
24. Junbom Kim, Seong-Min Lee and Supramaniam Srinivasan, *Electrochem. Soc*, 142(1995)2670.
25. G. Squadrito, G. Maggio, E. Passalacqua, F. Lufrano and A. Patti, *J Applied Electrochemistry*, 29 (1999) 1449.
26. Deryn Chu and Rongzhong Jiang, *J. Power Sources*, 80 (1999) 226.
27. Sossina M. Haile, *Acta. Materialia*, 51 (2003) 5981.
28. Bard AJ and Faulkner LR, *Electrochemical methods: fundamentals and applications*, 2nd edn. Wiley, New York (2000) .
29. Xiaozhi Yuan, Haijiang Wang, Jian Colin Sun and Jiujun Zhang, *Int. J. Hydrogen Energy*, 32 (2007) 4365.
30. Chien-Ming Lai, Jing-Chie Lin, Kan-Lin Hsueh, Chiou-Ping Hwang, Keh-Chyun Tsay, Li-Duan and Tsai, Yu-Min Peng, *Int. J. Hydrogen Energy*, 32 (2007) 4381.
31. Chien-Ming Lai, Jing-Chie Lin, Fu-Ping Ting, San-Der Chyou and Kan-Lin Hsueh, *Int. J. Hydrogen Energy*, 33 (2008) 4132.
32. Jing-Chie Lin, Chien-Ming Lai, Fu-Ping Ting, San-Der Chyou and Kan-Lin Hsueh, *J. Appl. Electrochem*, 39 (2009) 1067.
33. Mohammad Zhiani, Hussein Gharibi and Karim Kakaie, *Int. J. Hydrogen Energy*, 35 (2010) 9261.

34. Ning-Yih Hsu, Shi-Chern Yen, King-Tsai Jeng and Chun-Ching Chien, *J. Power Sources*, 161 (2006) 232.
35. S. A. Campbell, D. P. Wilkinson, M. Davis, J. St-Pierre and M. C. Johnson, *J. Electrochem. Soc.*, 144 (1997) 3845.